Letters

Graphene Nanofilms/Silicon Near-Infrared Avalanche Photodetectors

Lixiang Liu, Xiaoxue Cao, Xinyu Liu, Zhixiang Zhang, Xiaochen Wang, and Yang Xu, *Senior Member, IEEE*

Abstract—**Graphene/silicon Schottky junction diodes have been extensively studied and widely used in photodetection. However, limited to the low light absorption of single-layer graphene and bandgap of silicon, graphene/silicon devices exhibit low quantum efficiency in the infrared region. Here, we demonstrate a high-performance near-infrared Schottky diode by integrating silicon with the macroscopic assembled graphene nanofilms (nMAG). Because of the intense light absorption, low work function, and long carrier lifetime of nMAG, the device shows a detection spectra range up to 1870 nm with the responsivity of 0.4 mA/W and response speed of 371 ns. By driving the device into avalanche multiplication, 10^4-10^5 of avalanche gain has been obtained, and the responsivity at 1870 nm increases to 10 A/W. The device structure in this report could be compatible with the semiconductor process so that silicon-based infrared photodetectors with high performance and low cost could be potentially realized.**

Index Terms—**Graphene nanofilm, schottky junction, infrared, photodetector, avalanche.**

I. INTRODUCTION

THE photodetector is an essential tool for exploring the unknown world and fields, where it performs optical-to-electrical signal conversion [1]. Especially, infrared (IR) photodetector is the building block of an optoelectronic link in many vital fields, such as communication, imaging, aerospace, medical and military [2]–[4]. Various IR photodetectors developed from narrow-band-gap semiconductors (PbS, InSb, InGaAs, and HgCdTe) have shown outstanding responsivity, quantum efficiency, speed, and spectra range [5]. However, these photodetectors have struggled to meet the growing demands for compatibility of complementary metal-oxide−semiconductor (CMOS) and room temperature. Hence, the development of silicon (Si) photodetectors based on mature CMOS technology is essential for monolithic optoelectronic integration [6]. Si electronics has experienced revolutionary advancements through miniaturization and on-chip integration in the past six decades. While Si-based photodetectors are widely employed in the visible spectra range (400–700 nm) and are not suitable to cover short-wave and mid-wave infrared radiation above 1.1 μm [4].

Compared with metal materials, graphene attracts much attention in the photodetection domain because of its outstanding optical and electronic properties: high conductivity and mobility [7], the zero bandgap structure [8], long hot carrier relaxation time [9], and good compatibility with silicon-based processes [10], [11]. Graphene-based heterojunctions show promise for new generation IR photodetectors. However, caused by its monoatomic layer structure, graphene shows a low light absorption of 2.3% [12], which results in low hot carrier density and hence low quantum efficiency, especially in the IR region. Some strategies increase the light absorption of graphene optoelectronic devices [13]–[16], sacrificing the broadband property. A possible solution is to use multilayer graphene instead of single-layer (SLG) to increase light absorption.

Here, we prepared highly crystalline macroscopic assembled graphene nanofilms (nMAG) with uniform and tuned thicknesses, which show enhanced light absorption and a long hot carrier lifetime from the visible to mid-IR range [16]. By combining nMAG with Si into the Schottky diode, the Schottky barrier height (SBH) is reduced to 0.3 eV because of the lower work function (4.52 eV) of nMAG [17]. A low SBH is favorable for IR thermionic emission and expands the response band from 1342 nm to 1870 nm compared with SLG/Si diode. The device fabricated owns a photo responsivity of 0.4 mA/W at 1870 nm (bias voltage of -1 V) and a rising time of 317 ns. Moreover, by applying a significant reverse bias and driving nMAG/Si device to avalanche multiplication, the responsivity can be further increased up to 10 A/W at 1870 nm wavelength at -80 V, and the avalanche multiplication gain is about 10^4-10^5. The nMAG/Si photodetector provides a simple, cheap, and easy-processed approach for high responsivity, speed, and multiplication gain in the near-IR spectral range. It paves the way for graphene/Si optoelectronic integration.

II. DEVICE ARCHITECTURE

A. Device Fabrication

The device was fabricated on a commercial lightly-doped n-type Si wafer (doping concentration of 10^{15} cm^{-3} and resistivity of 1–10 Ω·cm) with a 100 nm SiO$_2$ layer. 1) Metal electrodes fabrication: The SiO$_2$ layer was patterned by photolithography

The authors are with the School of Micro-nanoelectronics, State Key Laboratory of Silicon Materials, Hangzhou Global Scientific and Technological Innovation Center, ZJU-UIUC Joint Institute, Zhejiang University, Hangzhou 310027, China (e-mail: 11731032@zju.edu.cn; 11931058@zju.edu.cn; xinyu_liu@zju.edu.cn; zhangzhixiang@zju.edu.cn; xiaochenwang@zju.edu.cn; yangxu-isee@zju.edu.cn).
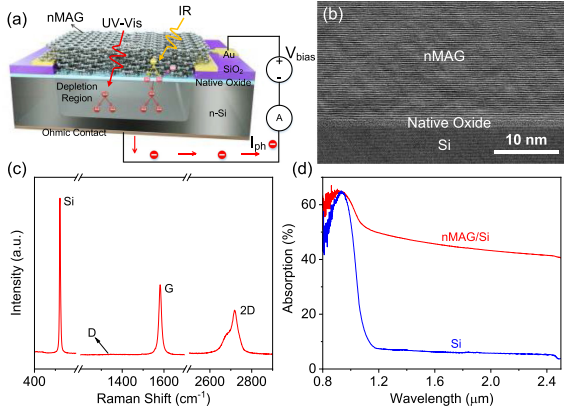
Fig. 1. The device structure of nMAG/Si. (a) The schematic of the nMAG/Si device. (b) The HR-TEM cross-sectional image of the nMAG/Si interface. (c) The Raman spectra of nMAG (Si substrate). (d) The absorption spectra of the nMAG/Si device.
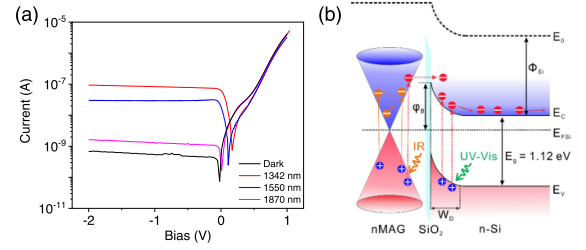

Fig. 2. (a) The I-V curves of the nMAG/Si device at different wavelengths with the same incident power (10 mW). (b) The energy band diagram structure of the nMAG/Si diode.

first. Then, the e-beam deposition process was used to deposit Cr/Au film as the electrodes, followed by the lift-off process. The thicknesses of the Cr and Au were 15 and 80 nm. 2) Silicon window etching: second photolithography was used to pattern silicon windows with the size of $500 \times 500 \ \mu m^2$. SiO_2 in the window was subsequently etched away by buffered oxide etchant. 3) nMAG transfer on Si window [16], [17]. The nMAG was directly transferred onto the Si window by tweezers, and the gap between nMAG and Si was then filled with deionized water. Nitrogen blowing on nMAG was used to unfold the wrinkles. 4) Ohmic contact preparation: GaIn was smeared to form Ohmic contact between Si substrate and copper tape at the backside. 5) Wire-bonding the device on PCB board.

B. Characterizations and Measurements

Raman spectroscopy of nMAG on Si substrate was conducted using RENISHAW RM2000 with a 532 nm laser. TEM images were acquired on a Hitachi H-9500 instrument operating at 300 kV. The absorption spectra were obtained by a Fourier Transform Infrared Spectroscopy (FT-IR) (Nicolet iN10, Thermofisher Scientific). The I-V curves were collected from Keithley Semiconductor Analyzer 2460. The time response curves were obtained by connecting the device and the trans-impedance amplifier (DHPCA-100, FEMTO, 200 MHz bandwidth) with an oscilloscope (Keysight DSO 9404A, 4 GHz bandwidth). The pulsed laser was triggered by TTL connecting with a signal generator. Agilent Semiconductor Analyzer B1500 applied the high reverse biases.

III. RESULTS AND DISCUSSION

Fig. 1(a) shows the schematic structure of the nMAG/Si device. In this structure, the 45 nm-thick free-standing nMAG was transferred onto the Si window ($500 \ \mu m \times 500 \ \mu m$) without metallic and polymer contaminations. The high-resolution transmission electron microscopy (HR-TEM) in Fig. 1(b) demonstrates that nMAG contacts well with the Si substrate. There is a thin (~2 nm) native oxide SiO_2 layer in the interface, which can depress the dark current without affecting the photocurrent

[18], [19]. Raman spectroscopy is employed to characterize the structural properties of nMAG in Fig. 1(c). The negligible D peak at 1330 cm^{-1} indicates a defect-free lattice structure [16]. Near-IR absorption spectrum (0.8-2.5 μm) of nMAG/Si is shown in Fig. 1(d). Notably, the absorption of Si substrate sharply decreases beyond 1.1 μm because of the bandgap of Si (1.12 eV). However, by combining nMAG with Si, the light absorption increases to 40% over a relatively broad wavelength range, almost 20 times that of SLG (2.3%). The enhanced light absorption contributes to the large density of photo-induced carriers in a broadband range.

The nMAG/Si device exhibits photoresponse in 1342–1870 nm. Fig. 2(a) shows the dark current and photocurrent as bias voltage varies from -2 to 1 V, exposure under laser beams of 1342 nm, 1550 nm, and 1870 nm with the same incident power of 10 mW (laser point diameter is 2 mm). A typical Schottky diode rectification behavior is observed, and the photoresponse decreases with wavelength increasing. To quantitatively analyze the device characteristic, we used the thermionic emission model [20]:

$$I = AA^*T^2 exp\left(-\frac{q\phi_B}{k_BT}\right)\left[exp\left(\frac{qV}{nk_BT}-1\right)\right] \quad (1)$$

Where A is the effective junction area, A^* is the Richardson constant of Si, q is the basic electric charge, ϕ_B is the SBH of the nMAG/Si junction, k_B is the Boltzmann constant, n is the ideal factor, T is the temperature, and V is the applied voltage. The SBH extracted from the diode's forward dark current-voltage (I-V) characteristics is 0.3 eV. The lower work function of nMAG (4.5 eV) than SLG (4.7 eV) leads to lower SBH when integrated with Si. The 0.3 eV SBH corresponds to a cut-off wavelength of 2.1 μm, considering the intrinsic Fermi level and symmetric Dirac band structure of nMAG, Fig. 2(b). For the wavelength $\leq$1.1 μm, the photons with energy higher than the Si bandgap can be absorbed by the Si substrate and excite electron-hole pairs in Si. The depletion region in Si can separate the electron-hole pairs directly to form photocurrent. While for the photon energy of $h\nu < E_g$ but $0.5h\nu > $ SBH (wavelength from 1.1 to 2.1 μm), the photon energy is insufficient to excite Si carriers. Photo-excited electrons in nMAG directly transfer over the barrier to Si and contribute to the photocurrent through the internal photoemission (IPE) effect [21]. When increasing the wavelength above 2.1 μm, the energy of photo-excited electrons
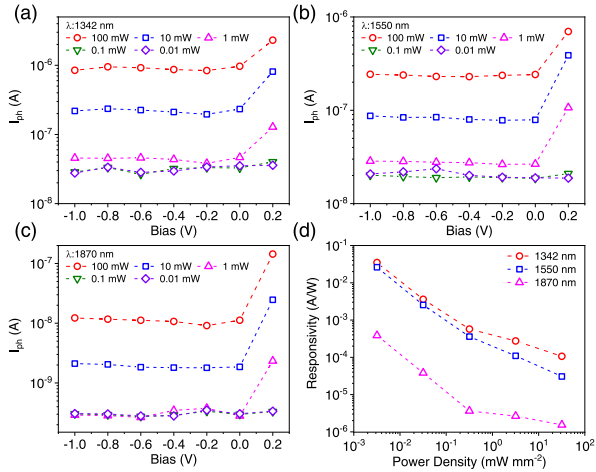
Fig. 3. The relationship between photocurrent and bias under different incident power at (a) 1342 nm, (b) 1550 nm, and (c) 1870 nm. (d) The responsivity of nMAG/Si as a function of incident power density at a different wavelength.
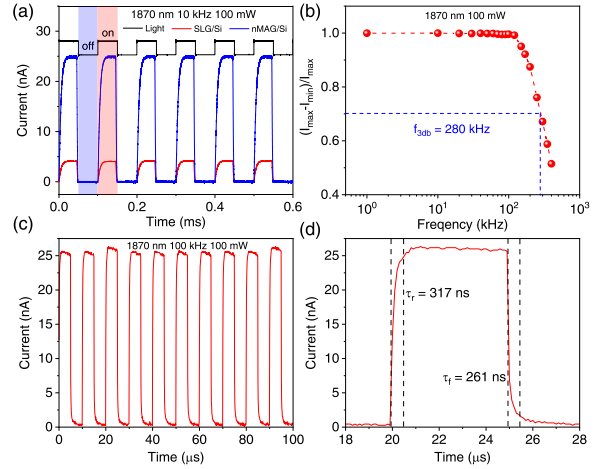

Fig. 4. The time response of nMAG/Si. (a) The time-dependent photocurrent of nMAG/Si at 1870 nm. (b) The normalized response as a function of light frequency from 1 Hz to 400 kHz. (c) The time-dependent photocurrent of nMAG/Si at 1870 nm with a power of 100 mW under 100 kHz light repetition. (d) The rising and falling time extraction from (c).

is lower than the SBH ($0.5h\nu <$ SBH), so almost no electrons jump through the barrier by the IPE effect.

Fig. 3(a)–(c) illustrate the photocurrent measured by the lock-in amplifier at different wavelengths with incident power varying from 0.01 to 100 mW. The photocurrent increases significantly as the power increases at the reverse bias. Responsivity is the key figure-of-merit parameter of a photodetector that reflects the photoelectric conversion capability of the device and is given by $R = \frac{I_{ph}}{P_{in}} = \frac{I_{light} - I_{dark}}{P_{in}}$. Fig. 3(d) shows the responsivity of the device under different wavelengths and incident power. Here, we get responsivity of 35 mA/W at 1342 nm wavelength and 0.4 mA/W at 1870 nm wavelength, and the responsivity increases with the light power decrease. The responsivity for nMAG/Si device is relatively low compared to quantum dots enhancement structures [22], but using the simple CMOS compatible Schottky diode structure and the intrinsic properties of nMAG is a promising way to expand the detection range of Si-based detector. By reducing the effective area of the device, we can depress the dark current and device noise and increase the response speed. What's more, by applying a significant reverse bias to the device, the avalanche multiplication effect will increase the light responsivity, which will be discussed later.

The light's varied pulsed frequency is used to examine response speed under TTL modulated light illumination. As shown in Fig. 4(a), distinguished on/off states can be observed from the time response curve at 1870 nm with a power of 100 mW under 10 kHz light repetition. Compared with nMAG/Si devices, SLG/Si shows a low photocurrent, almost one order of magnitude lower than nMAG/Si. The IR response of SLG/Si comes from the interfacial states between SLG and Si [23], considering the low light absorption and high work function of SLG. Fig. 4(b) shows the normalized photocurrent at different light frequencies, from which the 3-dB bandwidth is estimated to be 280 kHz, which indicates that the nMAG/Si device can follow the pulsed frequency of the light.

For a typical graphene/Si Schottky diode, the response time consists of carrier diffusion and drift time, and the parasitic

circuit time constant [24], which is about 3.2 ns theoretically [18]. Hence, to increase the response speed of the nMAG/Si device, we use a high-speed TTL-laser and trans-impedance amplifier to do the measurement. Fig. 4(c) and (d) present the periodic response at 1870 nm with the power of 100 mW under 100 kHz light repetition, and the rising time τ_r is estimated at ~317 ns, while the decay time τ_f is estimated at ~261 ns. Anyway, the response speed of nMAG/Si is limited by an external circuit and slow diffusion in bulk Si substrate.

Finally, to increase the IR light response of nMAG/Si, we drive the junction into an avalanche by applying a large reverse bias to -90 V. The electrons impact with other electrons in the high electric field of Si, generating plenty of new carriers and hence amplifying the signal [25]. Here, we fabricate the avalanche diode devices using Si substrate with a resistivity of 1000 $\Omega \cdot$cm instead of 1–10 $\Omega \cdot$cm as previously mentioned to gain a wider Si depletion region. Fig. 5(a) simply illustrates the avalanche processes in nMAG/Si: 1) nMAG absorbs IR light and generates electron-hole pairs, 2) electrons with energy higher than SBH inject into Si, 3) injected electrons gain high kinetic energy and collide with other carriers under high electric field in the depletion region, 4) mass new carriers generate. Fig. 5(b) shows the dark and photocurrent I-V curves with avalanche multiplication processes at 1870 nm wavelength varying incident power. With the increase of reverse bias, the leakage current increases. When the bias reaches -80 V, an avalanche happens under dark conditions, and there is a sharp increase in the current. Moreover, the voltage of the avalanche decreases with the incident power increasing, which donates more injected electrons for the avalanche in Si.

Fig. 5(c) is the calculated avalanche gain of the device. The calculation formula for avalanche gain is $M = \frac{I_{ph|V}}{I_{0|V_0}}$, Where $I_{ph|V}$ is the photocurrent at a reverse bias of V, $I_{0|V_0}$ is the dark current before avalanching at a reverse bias of -1V. The photocurrent contributes to the gain before the avalanche, while the multiplication current dominates the gain after the avalanche
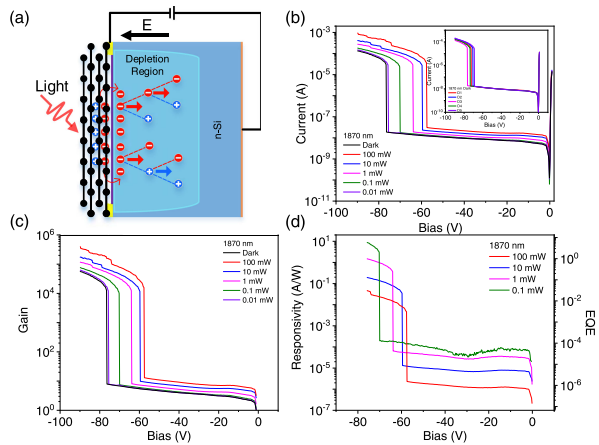
Fig. 5. The avalanche multiplication response of nMAG/Si. (a) The schematic of the avalanche multiplication processes in nMAG/Si. (b) The I-V curves of the nMAG/Si device (inset: the repeatability performance of different devices). (c) The calculated avalanche multiplication gain as a function of bias voltage. (d) the calculated responsivity and external quantum efficiency (EQE) as a function of bias voltage.

happens. We realize 4-5 orders of photocurrent increasing and get 10^4-10^5 multiplication gain after avalanche at 1870 nm wavelength with different light power. In addition, the calculated responsivity reaches 10 A/W under -80 V voltage with an incident power of 0.1 mW at 1870 nm, as shown in Fig. 5(d), which improves a lot compared with the responsivity of 0.4 mA/W at -1 V (before the avalanche, in Fig. 3(d)). It is a great improvement for graphene/Si-based photodetectors to reach high responsivity.

IV. CONCLUSION

In summary, a silicon-based near-infrared photodetector combined with nMAG has been demonstrated, which shows superior performance in terms of relatively broad spectra (1342–1870 nm), high responsivity (0.4 mA/W at 1870 nm before avalanche, 10 A/W after avalanche) and high speed (317 ns rising time). Importantly, high avalanche gain (10^4-10^5) is obtained by applying a large reverse bias to the device. The high light absorption, low work function, and long carrier lifetime of nMAG contribute to the response in the IR region, and the avalanche multiplication effect in Si contributes to the high responsivity of nMAG/Si. Moreover, since Si-based avalanche photodetectors are already well developed, the nMAG/Si photodetector, if operating in Geiger mode, may be able to detect single photons under the avalanche gain mechanism. This work provides a new path for developing Si-based IR photodetectors without external enhancement schemes and a complex preparation process.

ACKNOWLEDGMENT

REFERENCES

[1] I. Goykhman *et al.*, "On-chip integrated, silicon-graphene plasmonic Schottky photodetector with high responsivity and avalanche photogain," *Nano Lett.*, vol. 16, no. 5, pp. 3005–3013, May 2016.

[2] A. Erfanian, H. Mehrara, M. Khaje, and A. Afifi, "A room temperature 2 × 128 PtSi/Si-nanostructure photodetector array compatible with CMOS process," *Sensor Rev.,* vol. 35, no. 3, pp. 282–286, Jul. 2015.

[3] T. Yamazato *et al.*, "Image-sensor-based visible light communication for automotive applications," *IEEE Commun. Mag.*, vol. 52, no. 7, pp. 88–97, Jul. 2014.

[4] U. Willer, M. Saraji, A. Khorsandi, P. Geiser, and W. Schade, "Near- and mid-infrared laser monitoring of industrial processes, environment and security applications," *Opt. Lasers Eng.*, vol. 44, no. 7, pp. 699–710, Jul. 2006.

[5] P. Martyniuk, J. Antoszewski, M. Martyniuk, L. Faraone, and A. Rogalski, "New concepts in infrared photodetector designs," *Appl. Phys. Rev.*, vol. 1, no. 4, Dec. 2014, Art. no. 041102.

[6] T. R. Graham, *Silicon Photonics: The State of the Art.* Chichester; Hoboken, NJ, USA: Wiley, 2008.

[7] L. Banszerus *et al.*, "Ultrahigh-mobility graphene devices from chemical vapor deposition on reusable copper," *Sci. Adv.*, vol. 1, no. 6, Jul. 2015, Art. no. e1500222.

[8] K. S. Novoselov *et al.*, "Electric field effect in atomically thin carbon films," *Science*, vol. 306, no. 5696, pp. 666–669, Oct. 2004.

[9] M. W. Graham, S.-F. Shi, D. C. Ralph, J. Park, and P. L. McEuen, "Photocurrent measurements of supercollision cooling in graphene," *Nature Phys.*, vol. 9, no. 2, pp. 103–108, Feb. 2013.

[10] A. Pospischil *et al.*, "CMOS-compatible graphene photodetector covering all optical communication bands," *Nature Photon.*, vol. 7, no. 11, pp. 892–896, 2013.

[11] S. Goossens *et al.*, "Broadband image sensor array based on graphene-CMOS integration," *Nature Photon.*, vol. 11, no. 6, pp. 366–371, Jun. 2017.

[12] F. H. L. Koppens, T. Mueller, P. Avouris, A. C. Ferrari, M. S. Vitiello, and M. Polini, "Photodetectors based on graphene, other two-dimensional materials and hybrid systems," *Nature Nanotechnol.*, vol. 9, no. 10, pp. 780–793, Oct. 2014.

[13] G. Konstantatos *et al.*, "Hybrid graphene-quantum dot phototransistors with ultrahigh gain," *Nature Nanotechnol.*, vol. 7, no. 6, pp. 363–368, Jun. 2012.

[14] S. C. Du *et al.*, "Graphene/silicon-quantum-dots/Si Schottky-PN cascade heterojunction for short-wavelength infrared photodetection," in *Proc. 63rd IEEE Annu. Int. Electron. Devices Meeting*, San Francisco, CA, USA, 2017, pp. 8.7.1–8.7.4.

[15] X. M. Wang, Z. Z. Cheng, K. Xu, H. K. Tsang, and J. B. Xu, "High-responsivity graphene/silicon-heterostructure waveguide photodetectors," *Nature Photon.*, vol. 7, no. 11, pp. 888–891, Nov. 2013.

[16] L. Peng *et al.*, "Multifunctional macroassembled graphene nanofilms with high crystallinity," *Adv. Mater.*, vol. 33, no. 49, Dec. 2021, Art. no. 2104195.

[17] L. Peng *et al.*, "Macroscopic assembled graphene nanofilms based room temperature ultrafast mid-infrared photodetectors," *InfoMat*, vol. 4, no. 6, 2022, Art. no. e12309.

[18] X. Wan *et al.*, "A self-powered high-performance graphene/silicon ultraviolet photodetector with ultra-shallow junction: Breaking the limit of silicon?," *npj 2d Mater. Appl.*, vol. 1, pp. 1–8, Apr. 2017.

[19] L. Liu *et al.*, "Macroscopic-assembled-graphene nanofilms/germanium broadband photodetectors," in *Proc. IEEE Int. Electron. Devices Meeting*, San Francisco, CA, USA, 2021, pp. 9.2.1–9.2.4.

[20] S. K. Cheung and N. W. Cheung, "Extraction of Schottky diode parameters from forward current-voltage characteristics," *Appl. Phys. Lett.*, vol. 49, no. 2, pp. 85–87, 1986.

[21] M. Casalino, "Internal photoemission theory: Comments and theoretical limitations on the performance of near-infrared silicon Schottky photodetectors," *IEEE J. Quantum Electron.*, vol. 52, no. 4, Apr. 2016, Art. no. 4000110.

[22] T. Yu, F. Wang, Y. Xu, L. L. Ma, X. D. Pi, and D. R. Yang, "Graphene coupled with silicon quantum dots for high-performance bulk-silicon-based Schottky-junction photodetectors," *Adv. Mater.*, vol. 28, no. 24, pp. 4912–4919, Jun. 2016.

[23] W. Liu *et al.*, "Light-induced negative differential resistance in gate-controlled graphene-silicon photodiode," *Appl. Phys. Lett.*, vol. 112, no. 20, May 2018, Art. no. 201109.

[24] Y. A. Goldberg, "Semiconductor near-ultraviolet photoelectronics," *Semicond. Sci. Technol.*, vol. 14, no. 7, pp. R41–R60, 1999.

[25] Y. Kang *et al.*, "Monolithic Germanium/silicon avalanche photodiodes with 340 GHz gain-bandwidth product," *Nature Photon.*, vol. 3, no. 1, pp. 59–63, Jan. 2009.